

This is the accepted manuscript of the contribution published as:

Averbeck, M., **Kuhn, S.**, Bühligen, J., Götte, M., Simon, J.C., **Polte, T.** (2017):
Syndecan-1 regulates dendritic cell migration in cutaneous hypersensitivity to haptens
Exp. Dermatol. **26** (11), 1060 – 1067

The publisher's version is available at:

<http://dx.doi.org/10.1111/exd.13374>

DR. MARCO AVERBECK (Orcid ID : 0000-0002-0246-7646)

Article type : Regular Article

Syndecan-1 regulates dendritic cell migration in cutaneous hypersensitivity to haptens

Marco Averbeck^{1,#}, Stephanie Kuhn³, Johannes Bühligen¹, Martin Götte², Jan C. Simon^{1*}, and Tobias Polte^{1,3,*}

¹ Department of Dermatology, Venerology and Allergology, Universitätsklinikum Leipzig, Leipzig Germany

² Department of Gynecology and Obstetrics, Münster University Hospital, Münster, Germany

³ UFZ – Helmholtz Centre for Environmental Research Leipzig-Halle, Department of Environmental Immunology

* both authors contributed equally

#Corresponding author:

Marco Averbeck

Department of Dermatology, Venerology and Allergology,

This article has been accepted for publication and undergone full peer review but has not been through the copyediting, typesetting, pagination and proofreading process, which may lead to differences between this version and the Version of Record. Please cite this article as doi: 10.1111/exd.13374

This article is protected by copyright. All rights reserved.

Accepted Article

Leipzig University Medical Center

Philipp-Rosenthal-Str. 23

04103 Leipzig

Germany

Phone: + 49 341 97 18600

Fax: + 49 341 97 18609

e-mail: maverbeck@hautarztzentrum.de

Abstract

In human dendritic cells (DC), we previously demonstrated in vitro that syndecan-1 (SDC1) is downregulated during maturation correlating with enhanced motility.

We investigated the effects of SDC1 on DC migration in vivo during TNCB(2,4,6-trinitro-1-chlorobenzene)-induced cutaneous hypersensitivity reaction (CHS) in mice.

We show that DC in SDC1-deficient mice migrated faster and at a higher rate to lymph nodes draining the hapten-painted skin. Adoptive transfer of SDC1-deficient hapten- and fluorochrome-labelled DC into wild type (WT) mice led to increased and faster migration of DC to paracortical lymph nodes, and to a stronger CHS compared to WT DC. In SDC1^{-/-} mice, CCR7 remains longer on the DC surface within the first 15 min maturation (or: after LPS-induced maturation). In addition, a time-dependent up-regulation of CCL2, CCL3, VCAM1 and talin was found during maturation in SDC1^{-/-} DC. However, no difference in T cell stimulating capacity of SDC1-deficient DC was found compared to WT DC. Mechanistically, SDC1-deficient DC showed enhanced migration towards CCL21 and CCL19. This may result from functional overexpression of CCR7 in SDC1^{-/-} DC. Increased and accelerated migration of otherwise functionally intact SDC1-deficient DC leads to an

This article is protected by copyright. All rights reserved.

exacerbated CHS. Based on our results, we conclude that SDC1 on DC negatively regulates DC migration.

Short title: Syndecan-1 affects Dendritic cell migration

Key words: dendritic cell, cell migration, syndecan, cutaneous hypersensitivity,

Abbreviations: CFDA = 5-(and -6)-carboxyfluorescein diacetate succinimidylester, CHS=contact hypersensitivity, DC = dendritic cell, DTH = delayed-type hypersensitivity, TRITC = tetramethylrhodamine, SDC1 = syndecan-1, WT = wild-type, TNCB= 2,4,6-trinitro-1-chlorobenzene

Introduction

Dendritic cells (DC) in the skin act as sentinels of the immune system (1, 2). During microbial invasion or allergen contact, immature DC receive simultaneous activation signals through the binding of conserved molecular motifs by pattern recognition receptors, such as Toll-like receptors (TLR) and C-type lectin receptors (3). This results in DC maturation and migration to secondary lymphoid organs, where DC present the processed antigens to naive T cells and induce antigen-specific immune responses (4).

DC migration is a complex process which requires a time and place dependent regulation of adhesion structures and cytokines to mobilize DC in the extracellular matrix and to direct DC into lymphatic tissues (5) (6). Directional DC migration is mainly controlled by chemokines CCL21 and CCL19 which are expressed on lymphatic endothelia and in T cell rich regions in the lymphatic tissues and bind to upregulated CCR7 on mature DC (7). Additionally, chemokines may bind to co-receptors like heparan sulfate as this is the case for CCL21 (8).

Binding of chemokines to heparan sulfate proteoglycans may force chemokines to oligomerize and thus increase chemosensitivity of cells (9, 10).

The syndecan (SDC) family of cell surface heparan sulfate proteoglycans is important in the regulation of inflammation. Bearing heparan sulfate chains, SDC interact with a multitude of extracellular ligands important in driving inflammation, e.g. chemokines and their receptors (11-13). SDC1 is expressed in epithelia, endothelia, and several leukocyte subgroups including pre-B cells, DC and macrophages. SDC1-deficient mice show an increased inflammation in oxazolone-induced DTH (14). This was ascribed to an increased leukocyte recruitment following elicitation of DTH due to increased ICAM-1-mediated adhesion. However, the role of DC during DTH was not addressed. In human monocyte-derived DC SDC1 is downregulated during maturation correlating with enhanced DC motility (15). In this paper we wished to elucidate the role of SCD1 for DC migration in vivo and its impact on the regulation of cutaneous immune responses.

Methods

Mice

Syndecan-1 knockout (SDC1^{-/-}) mice on a C57BL/6J background (16) that had been backcrossed for 11 generations and their WT counterparts were bred, housed, and handled according to the guidelines the Committee on Animal Welfare of Saxony.

CHS

Sensitisation was performed by painting 7% TNCB (Sigma-Aldrich) in olive oil of shaved abdomen of WT or SDC1^{-/-} mice. Challenge was done 5 days later by application of 1% TNCB to both sides of the left ear of the mice; the right ear was treated with olive oil for control. 1% TNCB application without prior sensitisation did not induce significant ear

swelling (data not shown). After 3h, 6h and 24h measurement of the ear swelling of left and right ear was performed using a digital caliper. Right ear thickness was subtracted as baseline, respectively and compared to WT mice with prior application of olive oil to the abdomen. Analysis of DC migration during DTH sensitization was performed by TRITC (100µl TRITC and DMSO in Acetone and Dibutylphthalate) painting (Molecular Probes) to the shaved abdomen 12h, 24h or 48h prior to LN extraction. The amount of DC migrated into inguinal LNs from abdominal skin was detected by FACS analysis of DC carrying TRITC and CD11c.

Bone marrow derived DC were generated by harvesting bone marrow from the tibia and femur of WT or SDC1^{-/-} mice. The cells were re-suspended at 1x10⁶ cells/ml in cRPMI (Gibco) containing 40 ng/ml GM-CSF and 100 ng/ml IL-4 (both PromoCell, Germany). Cells were fed on days 3 and 5 of culture by replacing half the medium in each well with fresh cRPMI containing GM-CSF and IL-4. Murine CD11c⁺ cells were separated by using magnetic cell sorting systems and CD11c Microbeads (Milteny Biotec, Bergisch Gladbach, Germany).

Bone marrow derived DCs from WT and SDC1^{-/-} mice were pulsed in vitro with 1 mM TNBS at 37°C for 7 minutes. For analysis of DC migration by adoptive transfer 600.000 CFDA-stained and/or TNBS-pulsed WT or SDC1^{-/-} DC were injected into the footpads of WT or SDC1^{-/-} mice. LNs were extracted, and CFDA⁺ CD11c⁺ DC were quantified by flow cytometry out of a total of 10.000 cells from each LN following 12h, 24h or 48h after adoptive transfer. Otherwise the mice were challenged 5 days later by application of 1% TNCB and ear swelling was measured as described above.

Flow cytometric analysis

Cells were measured on BD FACS Canto II (BD Biosciences Pharmingen, Heidelberg, Germany) and experiments were analyzed with FACS DIVA and FlowJo software. Dead cells were excluded from analysis by staining with fixable viability dye eFluor® 450 (eBioscience). The following isotype controls and anti-mouse antibodies were purchased from BD: rat IgG1-PE (R3-34), CD80-PE (16-10A1), CD86-PE (GL1), Syndecan-1-PE. CCR7-Biotin (4B12) and CCR7 PerCP-Cy5.5 were from Miltenyi and Biolegends, respectively. For extracellular CCR7 staining cells were harvested, washed with PBS and stained with CCR7 antibody or isotype control for 10 min at 37°C. Subsequently, cells were incubated for further 30 min at room temperature. Intracellular CCR7 staining: after regular extracellular staining, cells were fixed with 4% PFA in PBS for 5 min at RT, washed with PBS and permeabilized with 0.5% saponine buffer for 10 min at RT. Subsequently, antibody or isotype control were added for further 30 min.

Histology

Normal and diseased ear tissue from WT and SDC1 ^{-/-} mice were cryoconserved and later on formalin-fixed and paraffin-embedded using standard techniques essentially as described by Staite *et al.*(17). Consecutive sections of 4 µm were cut from the paraffin blocks, dewaxed, and rehydrated and then H&E-stained. Sections were observed with an Olympus X71 microscope equipped with a Leica camera. Alternatively, cryosections were dried and blocked for 10 min with PBS containing 2% BSA and stained for CD11c (BD Biosciences) and DAPI (Molecular Probes). 48h following adoptive transfer of CFDA-labelled (see below) WT and SDC1^{-/-} DC cryosections (4 µm) of lymph node tissue from SDC1^{-/-} and WT mice were dried and blocked for 10 min with PBS containing 2% BSA. CFDA-positive cells were detected using TissueFAX™ and an overlay with a transmission image was generated.

Proliferation assay

Following sensitization of WT und SDC1^{-/-} mice and challenge after 5 days retroauricular LNs were obtained. T cells were labeled with 5 μ M of the intracellular fluorescent dye 5-(and -6)-carboxyfluorescein diacetate succinimidylester (CFDA, Molecular Probes) for 10 min and co-incubated with TNBS-pulsed or LPS-matured DC for the time points indicated, followed by analysis of the staining intensity by flow cytometry. LPS maturation of DC was performed as previously described (15).

Transwell migration assay

LPS (100ng/ml) matured 100.000 WT or SDC1^{-/-} DC were seeded into 24 plate transwells (Corning) and incubated over 4h in RPMI 1640 cell medium supplemented with, 1% L-glutamine (Seromed, Germany) and 0,5% fetal calf serum (FCS) with a tested endotoxin content lower than 1pg/ml (Promocell) and is referred to as. In some experiments, CCL19 or CCL21 (10ng/ml, PreproTech) were added as a chemotaxans to the lower chamber. DC that migrated through the transwell were acquired and quantified by flow cytometry.

qRT-PCR

Total cellular RNA was isolated using the rna-OLS Kit (OMNI Life Science, Hamburg, Germany) and reverse transcribed using the high capacity cDNA synthesis kit (Applied Biosystems). cDNA corresponding to 0.5 ng of total RNA was used as a template in the PCR consisting of Applied Biosystems MasterMix and predesigned TaqMan gene expression systems (Applied Biosystems) according to the manufacturer's instructions. For detection of CCL3/MIP-1, CCL2/MCP-1, Interferon-gamma, Interleukin (IL)-1beta, and VCAM-1, TaqMan probes Mm00441242_m1 (CCL2), Mm00441258_m1 (CCL3), Mm01168134_m1 (IFNG), Mm01336189_m1 (IL1b), and Mm00449197_m1 (VCAM) were used and normalized to the

Accepted Article

expression of beta-actin (Mm00607939_s1) (all primers from Applied Biosystems). Quantitative real-time PCR was performed with an Applied Biosystems PRISM 7300 Sequence Detection System by using the default thermal cycling conditions (10 min at 95°C and 40 cycles of 15 s at 95°C plus 1 min at 60°C). Relative quantitation was performed using the comparative cycle threshold method. For the detection of talin expression, SYBR-green-based PCRs were employed, using a cDNA equivalent of 50 ng total RNA as template in a total reaction volume of 20 µl with Power SYBR Green PCR mix (ABI) on an Step One Plus cycler (ABI) using the same cycling conditions. Primers were added at 0.375 µM each. Beta actin was used as a housekeeping gene for normalization. Primer sequences were (forward) 5'-AGGTGGTGTCCAACCTGAAG -3' and (reverse) 5'- CTGCAGGAGTTCTCGGACTG-3' for talin, and (forward) 5'-AGAGGGAAATCGTGCGTGAC -3' and (reverse) 5'-CAATAGTGATGACCTGGC CGT-3' for beta-actin. Specificity of amplification was controlled by melting curve analysis. Three to five biological replicates were used for each time point investigated.

Statistical analysis

Statistical analysis was performed using the Graphpad™ Prism software (Version 5.01 for Windows, GraphPad Software, San Diego California USA, www.graphpad.com). Only p-values below the significance level 0.05 (95% confidence interval) are indicated.

Results

SDC1^{-/-} DC migrate faster towards draining lymph nodes following antigen uptake

It has previously been shown that SDC1^{-/-} mice exhibit a stronger DTH. This was ascribed to a higher leukocyte adhesion, and a higher transmigration through the endothelial cell layer (14). On the other hand, DC migration from the skin into draining lymph nodes is a critical

step in DTH. Therefore, we wanted to investigate the in vivo migratory capacity of DC lacking SDC1. First, we could exclude differences in distribution of DC in skin and LN in SDC1^{-/-} compared to WT (data not shown). Likewise, no differences in the expression of several maturation markers (MHCII, CD86, CD11c) on SDC1^{-/-} vs WT DC were found in vitro, as well as in vivo (data not shown). Following the application of the fluorescent contact allergen tetramethylrhodamine (TRITC) on the shaved abdomen a higher number of CD11c/TRITC positive DC were detected in the strained draining inguinal lymph node of SDC1^{-/-} mice after 12h to 48h (Figure 1 A). However, the time courses of the detection of CD11c/TRITC-positive SDC1^{-/-} DC paralleled the time course of CD11c/TRITC-positive WT DC.

Antigens may arrive earlier in the lymph node than DC and the antigen might then be taken up by resident lymph node DC. Therefore, we performed adoptive transfers of fluorescently CFDA-labelled SDC1^{-/-} DC which were pulsed with the hapten TNBS. The CFDA-labelled SDC1^{-/-} DC were injected intracutaneously into the hind footpads of WT mice and strained draining inguinal lymph nodes were analysed for CFDA/CD11c-positive cells by FACS. Here, a higher number of SDC1^{-/-} DC were detected following a time course of 48h compared to adoptively transferred WT DC (Figure 1B). Again, the time course of SDC1^{-/-} DC paralleled the time course of WT DC. However, WT DC injected into SDC1^{-/-} mice reached the lymph nodes at lower numbers. Of note, the peak detection of DC following TRITC painting was after 12h while adoptively transferred DC peaked after 48h which most likely is due to a longer draining route of adoptively transferred DC injected into the footpad.

SDC1^{-/-} DC migrate into paracortical LN regions as WT DC

Analysis of cryosections of skin-draining lymph nodes by fluorescence microscopy revealed that the transferred SDC1^{-/-} DC located to the paracortical areas as do WT DC. Thus, SDC1^{-/-} DC migrate into DC innate areas. Again, an elevated number of migrated SDC1^{-/-} DC can be noted (Figure 1C).

SDC1^{-/-} DC are sufficient to elicit an increased CHS response in Mice

It has been previously shown that SDC1^{-/-} mice show an enhanced DTH reaction towards oxazolone (14). We could confirm this finding in another model using abdominal sensitization to TNCB. The histological sections of challenged ears of SDC1^{-/-} mice demonstrate increased edema formation and an increased lymphocytic infiltrate (Figure 2A). Specifically, SDC1^{-/-} mice showed an earlier DTH response after 3h and an overall increased response compared to WT mice after 24h (Figure 2B). To test, whether hypermigratory SDC1^{-/-} DC suffice to elicit an enhanced DTH response, isolated SDC1^{-/-} or WT DC were pulsed ex vivo with TNBS and adoptively transferred into WT mice. No differences in the expression of several maturation markers (CD86, CD80) on SDC1^{-/-} vs WT DC were found in vitro following TNBS (data not shown). Importantly, sensitization by SDC1^{-/-} DC led to an enhanced DTH response in WT mice (Figure 2C).

SDC1^{-/-} DC increase expression of CCL2, CCL3 and VCAM1 during maturation

First, to rule out non-specific inflammation in SDC^{-/-} mice we measured global inflammatory markers IL-6 and CRP in the serum. We could detect no differences in IL-6 and CRP serum levels between WT and SDC1^{-/-} mice in control as well as in TRITC treated animals (Figure 3A).

We found a time dependent regulation of the chemokines CCL2 and CCL3 in which CCL3 was significantly upregulated 3h following maturation in SDC1^{-/-} DCs. Likewise, CCL2 was significantly upregulated in SDC1^{-/-} DCs but 24h following maturation (Figure3B). VCAM1, an adhesion molecule, is higher expressed in SDC1^{-/-} DC which is pronounced during the first 3h of maturation (Figure 3B). Moreover, the expression of talin, a molecule pivotal in

inside-out-activation of integrins (18), was increased in SDC1^{-/-} DC compared to WT (Figure 3B). No differences in the expression of IL1- β and IFN- γ were observed (data not shown).

SDC1^{-/-} DC migrate faster towards CCL19 and CCL21

Heparan sulfate establish chemokine gradients and facilitate signaling via chemokine receptors, including CCL21 interaction with CCR7 (12, 19, 20). DC migration is heavily dependent on the interaction of the chemokine receptor CCR7 with its ligands CCL21 and CCL19 (Forster *et al.*, 1999;Schumann *et al.*, 2010). To test whether chemokine responsiveness is involved in the enhanced migratory capacity of SDC1-deficient DC we performed transwell experiments. Interestingly, mature SDC1^{-/-} DC displayed a significantly higher migration rate to CCL21 and CCL19 (Figure 4A). Furthermore, a significant different time course of CCR7 surface expression on SDC1^{-/-} DC was observed. We found higher extracellular CCR7 expression in SDC1^{-/-} mice 15 min after LPS activation compared to WT mice (Figure 4B). Since less CCR7 will be internalized in SDC1^{-/-} DCs following LPS maturation the ratio of extracellular to intracellular CCR7 expression was higher from 15 min to 3h . Thus, In SDC1^{-/-} CCR7 apparently remain longer on the DC surface after LPS treatment. The expression of CCR7 did not differ in SDC1-deficient or wildtype DC following 24h (Figure 4B).

Since an increased cellular infiltrate in the TNCB challenged ears was noticed (Fig 2A), we tested whether SDC1^{-/-} DC might activate T cells from local draining LN of TNCB sensitized mice differently. Thus, T cells from TNCB sensitized mice were isolated and subsequently restimulated with TNBS-pulsed DC. Both, WT DC and SDC1^{-/-} DC activate T cells in a proliferation assay similarly, although a – statistically non-significant (Tukey multiple comparison test $p>0.05$) - trend of a more effective T cell activation following restimulation with TNBS pulsed SDC1^{-/-} DC (Figure 4C) was noted.

Discussion

Here we report that a lack of SDC1 on DC lead to a hypermigratory state resulting in their increased migration into draining lymphnodes following antigen contact and ultimately, to an enhanced CHS immune response. The results are consistent with the observation of enhanced leukocyte recruitment in SDC1^{-/-} mice (14, 21). These authors demonstrated that this was due in part to a more efficient interaction of ICAM-1 and its $\beta 2$ integrin counter receptor (14). CCL2 amplify and maintain inflammation through chemokine-cytokine networks after the recruitment of circulating leukocytes (22). In our study, the time-dependent upregulation of CCL2 and CCL3 during SDC1^{-/-} DC maturation may also be account for increased recruitment of leukocytes explaining the observed increased cellular infiltrate in the CHS reaction in SDC1^{-/-} mice (Figure 2A).

Here, we show that in addition an increased SDC1^{-/-} DC migration in matured and immature conditions *in vitro* towards CCL19 and CCL21 (Figure 3A). This is probably a result from a functional overexpression of CCR7 in SDC1^{-/-} DCs within the first 3h of maturation. However, a true higher extracellular disposability of CCR7 in SDC1^{-/-} DCs is found only 15min following maturation (Figure 4B). If a longer persistence of CCR7 on SDC^{-/-} DCs surface is causative by a change of the pericellular glycosaminoglycan coat remains to be elaborated. Alternatively, different desensitisation mechanisms of the G-protein-coupled-receptor CCR7 such as endocytosis or oligomerisation may be influenced by the lack of heparan sulfate and chondroitin sulfate from adjacent SDC1 (23). At least SDC4 has been shown to influence integrin recycling (24). A regulation of CCR7 signalling and endocytosis through sialysation has been shown recently (25). Finally, experiments using SDC1^{-/-} CCR7-

Accepted Article

/- double knock out DC migration towards CCL21 and CCL19 will answer definitively if upregulated CCR7 is causative for enhanced DC migration in the absence of SDC1.

Additionally, VCAM1 exhibit a higher expression on SDC1^{-/-} DC, which is also more pronounced during the first 3h of maturation. VCAM1 mediates endothelial adhesion via integrin binding (26). Thus, a combined effect of increased CCR7 mediate chemotaxis and increased endothelial integrin binding may allow for the more potent SDC1^{-/-} DC migration. Moreover, the upregulation of talin, a molecule involved in inside-out-activation of integrins (18) in SDC1^{-/-} DC suggests that an enhanced integrin activation may have additionally contributed to the enhanced DC motility in these cells. Indeed, CCR7-dependent activation of DC integrins has been previously discussed as a mechanism promoting mobilization of antigen-charged DCs (27).

However, pericellular chondroitin sulfate on DC is also provided by other chondroitin sulfate bearing proteins like other SDCs (e.g. SDC4) or CD44. At least on (lymphatic) endothelial cells, heparan sulfate establishes chemokine gradients and facilitates signaling via chemokine receptors, including CCL21 interaction with CCR7 (12, 19, 20). Moreover, highly sulfated forms of chondroitin sulfate are capable of binding CCL21 (28), and SDC1 can be substituted with both heparan and chondroitin sulfate chains (29) in contrast to other syndecans. Moreover, binding of some cytokines to SDC-1 depends on the cooperation of heparan sulphate and chondroitin sulphate chains (Deepa *et al.*, 2004). Finally, it has to be noted that heparan sulfate structure varies in a cell-type-dependent manner, therefore, findings from endothelial and cancer cells may not be exactly comparable to DC (12). For example, heparin, which is more extensively sulfated compared to its structural homolog heparan sulfate, is able to interact with, and inhibit lymphocyte chemotaxis towards CCL21, but not CCL19 (30), whereas degradation of chondroitin sulfate affected DC migration towards both chemokines in our experimental system. Moreover, it has been shown that during experimental glomerulonephritis heparan sulfate fine structure differs between WT and SDC1^{-/-} mice at least in the glomerular endothelium (31).

Accepted Article

A haptotactic concept of directional migration of DC in skin has been established recently (32). Here, a gradient of CCL21 generated by lymphoendothelial cells guides DC to the lymph vessels. It is interesting to note that adoptively transferred WT DC into SDC1^{-/-} mice showed a markedly slower migration into the draining lymph nodes (Figure 1B). Possibly, high SDC1 expression in these cells might convey stationary characteristics or, more appealing, display themselves a haptotactic source for other cells. Furthermore, skin DC have opposite functions in CHS reaction, i.e. depending on the amount of antigen Langerhans cells sensitize at lower antigen concentration while at higher antigen concentrations Langerhans cells may have downregulatory functions (33). Presence of SDC1 on tumor cells seems to decrease their migratory capacity (34-36). For example, recent studies in SDC1-depleted breast cancer cells revealed that absence of SDC1 promoted the activity of beta-integrins and the activation of integrin-related signaling pathways, including focal adhesion kinase activation and Rho-GTPase-dependent cell motility (37, 38). Recent data in Jurkat T-cells suggest that another member of the Syndecan family, SDC2, blocks the active conformation of the leukocyte integrin LFA-1 (39). Considering the caveat that this modulation will depend on the individual integrin expression pattern of the SDC1-deficient cell type, and its surrounding matrix environment, similar mechanisms may play a role in DC (27, 40).

Since SDC1^{-/-} DC migrate into innate lymph node areas and T cell activation by SDC1^{-/-} DC is similar to WT DC, we conclude that the increased DTH response in SDC1-deficient mice is in a great part due to the higher migratory capacity of SDC1^{-/-} DC due to a functional overexpression of CCR7, and an increased expression of VCAM1 and talin. These findings corroborate the hypothesis that SDC1 reinforces tissue adherence of dendritic cells and thus weakens their capacity to sensitize to epicutaneously applied antigen.

Acknowledgements

This article is protected by copyright. All rights reserved.

M.A. was supported by the Berliner Stiftung für Dermatologie.

Figure Legends

Figure 1. SDC1^{-/-} DC migrate faster towards draining lymphnodes following antigen uptake

(A): Total cell counts of DC migrated into inguinal LN from abdominal skin. DC were carrying TRITC staining that was applied to the abdomen 12h, 24h or 48h prior to LN extraction. TRITC⁺ CD11c⁺ DC were acquired and quantified by flow cytometry out of a total of 10.000 cells from each LN. Grey boxes: WT DC, white circles: SDC1^{-/-} DC. Nine independent experiments were performed and analyzed each. Values are displayed as category graph peaks with lines indicating minimum and maximum. Area under the curve (AUC) for each paired experiment was calculated. The results are depicted in a column graph. P- Value result from a paired t-Test.

B) Total cell counts of DC migrated into inguinal LN 12h, 24h or 48h after adoptive transfer. 600.000 CFDA stained and TNBS treated WT or SDC1^{-/-} DC were injected into the footpads of WT or SDC1^{-/-} mice. LN were extracted, CFDA⁺ CD11c⁺ DC were acquired and quantified by flow cytometry out of a total of 10.000 cells from each LN. Grey boxes: WT DC, white circles: SDC1^{-/-} DC. Nine independent experiments were performed and analyzed each.

Values are displayed as category graph peaks with lines indicating minimum and maximum. Area under the curve (AUC) was calculated for each curve. Area under the curve (AUC) for each paired experiment was calculated. The results are depicted in a column graph. P- Value result from a one way ANOVA with Greenhouse-Geisser correction.

(C) SDC1^{-/-} DC migrate into paracortical LN regions as WT DC. DC migrated into inguinal LN 24h after adoptive transfer. 600,000 CFDA-stained and TNBS-treated WT or SDC1^{-/-} DC were injected into the footpads of WT or SDC1^{-/-} mice. LN were extracted and images of CFDA⁺ CD11c⁺ DC in cryo sections of LN were acquired by TissueFAX. Overlays of the fluorescent image and transmission image were done; dotted line highlight margins of paracortical zone in the transmission image.

Figure 2. SDC1^{-/-} DC are sufficient to elicit an increased DTH response in Mice

A) HE stainings of 4 μ m sections of ear skin 24h following 1%TNCB painting in sensitized mice as above (lower panel). Upper panel control ears painted with olive oil are displayed. B) 7% TNCB in olive oil was applied to the shaved abdomen of WT or SDC1^{-/-} mice. 5 days later 1% TNCB was applied to both sides of the left ear of the mice, the right ear was treated with olive oil for control. After 3h, 6h and 24h measurement of the ear swelling was performed and compared to control mice without prior application of TNCB to the abdomen. Grey boxes: WT mice, white circles: SDC1^{-/-} mice. Six independent experiments were performed and analyzed each. Values are displayed as category graph peaks with lines indicating minimum and maximum. Area under the curve (AUC) for each paired experiment was calculated. The results are depicted in a column graph. P- Value result from a paired t-Test. C) 600,000 TNBS-treated WT or SDC1^{-/-} DC were injected into the footpads of WT mice. 5 days later 1% TNCB was applied to both sides of the left ear of the mice, the right ear was treated with acetone/olive oil for control. After 3h, 6h and 24h measurement of the ear swelling was performed and compared to blank mice without prior application of TNBS-treated DC Grey boxes: WT mice, white circles: SDC1^{-/-} mice. Six independent experiments were performed and analyzed each. Values are displayed as category graph peaks with lines indicating minimum and maximum. Area under the curve (AUC) for each paired experiment was calculated. The results are depicted in a column graph. P- Value result from a paired t-Test.

Figure 3. SDC1^{-/-} DC increase expression of CCL2, CCL3, VCAM1 and talin during maturation

A) Serum from WT and SDC1^{-/-} mice was analyzed for global inflammatory markers CRP and IL-6 by ELISA. Values displayed as mean with SD in a column graph, n=8, WT black columns, SDC1^{-/-} grey column.

B) Time-dependent mRNA expression of CCL2, CCL3, VCAM1 and talin in lipopolysaccharide (LPS)-stimulated DCs was analysed by qRT-PCR. Values are displayed in a column graph as mean with SD. Black columns WT DC and grey columns SDC1^{-/-} DC. p-values result from paired t-Test, n=4.

Figure 4. SDC1^{-/-} DC migrate faster towards CCL19 and CCL21

A) Total cell counts of DC migrated through 8 μ m transwell plates. 100.000 WT or SDC1^{-/-} DC were seeded into 24 plate transwells and incubated over 4h. DC that migrated through the transwell were acquired and quantified by flow cytometry. Grey boxes: WT DC, white boxes: SDC1^{-/-} DC. Eight independent experiments were performed and analyzed each. Values are displayed as box (MM percentile) with a line indicating median values and whiskers from minimum to maximum. P-values result from ANOVA followed by Tukey's post hoc test. B) Intracellular and extracellular CCR7 expression of immature and LPS-matured WT and SDC1^{-/-} DC was analysed by FACS. A representative experiment at 15 min LPS maturation is depicted as dot plot left panel. Four independent experiments were done. The extracellular expression is depicted as column (mid panel) and the ratio of extracellular and intracellular CCR7 is displayed as category graph (right panel), peaks with lines indicating minimum and maximum. P- Value result from a paired t-Test. C) 7% TNCB in acetone/olive

oil was applied to the shaved abdomen of WT mice. 5 days later the LN were extracted and 100.000 CFDA stained T-cells each were incubated with 10.000 either non-stimulated, LPS stimulated or TNBS pulsed WT or SDC1 ^{-/-} DC. Proliferation was measured on day 7 by decrease of CFDA staining by flow cytometry. Grey boxes: WT DC, white boxes: SDC1 ^{-/-} DC. Five independent experiments were performed and analyzed each. Values are displayed as box (MM percentile) with a line indicating median values and whiskers from minimum to maximum.

References

1. Banchereau J, Steinman RM. Dendritic cells and the control of immunity. *Nature* 1998;**392**(6673):245-252.
2. Trombetta ES, Mellman I. Cell biology of antigen processing in vitro and in vivo. *Annu Rev Immunol* 2005;**23**:975-1028.
3. Geijtenbeek TB, van Vliet SJ, Engering A, t Hart BA, van Kooyk Y. Self- and nonself-recognition by C-type lectins on dendritic cells. *Annu Rev Immunol* 2004;**22**:33-54.
4. Noordegraaf M, Flacher V, Stoitzner P, Clausen BE. Functional redundancy of Langerhans cells and Langerin+ dermal dendritic cells in contact hypersensitivity. *J Invest Dermatol* 2010;**130**(12):2752-2759.
5. Kissenpfennig A, Henri S, Dubois B, Laplace-Builhe C, Perrin P, Romani N, et al. Dynamics and function of Langerhans cells in vivo: dermal dendritic cells colonize lymph node areas distinct from slower migrating Langerhans cells. *Immunity* 2005;**22**(5):643-654.
6. Schumann K, Lammermann T, Bruckner M, Legler DF, Polleux J, Spatz JP, et al. Immobilized chemokine fields and soluble chemokine gradients cooperatively shape migration patterns of dendritic cells. *Immunity* 2010;**32**(5):703-713.
7. Ohl L, Mohaupt M, Czeloth N, Hintzen G, Kiafard Z, Zwirner J, et al. CCR7 governs skin dendritic cell migration under inflammatory and steady-state conditions. *Immunity* 2004;**21**(2):279-288.
8. Yin J, Seeberger PH. Applications of Heparin and Heparan Sulfate Microarrays. 2010;**478**:197-218.
9. Handel TM, Johnson Z, Crown SE, Lau EK, Proudfoot AE. Regulation of protein function by glycosaminoglycans--as exemplified by chemokines. *Annu Rev Biochem* 2005;**74**:385-410.

10. Hoogewerf AJ, Kuschert GS, Proudfoot AE, Borlat F, Clark-Lewis I, Power CA, et al. Glycosaminoglycans mediate cell surface oligomerization of chemokines. *Biochemistry* 1997;**36**(44):13570-13578.
11. Bartlett AH, Hayashida K, Park PW. Molecular and cellular mechanisms of syndecans in tissue injury and inflammation. *Mol Cells* 2007;**24**(2):153-166.
12. Gotte M, Echtermeyer F. Syndecan-1 as a regulator of chemokine function. *ScientificWorldJournal* 2003;**3**:1327-1331.
13. Kumar AV, Katakam SK, Urbanowitz AK, Gotte M. Heparan sulphate as a regulator of leukocyte recruitment in inflammation. *Curr Protein Pept Sci* 2015;**16**(1):77-86.
14. Kharabi Masouleh B, Ten Dam GB, Wild MK, Seelige R, van der Vlag J, Rops AL, et al. Role of the heparan sulfate proteoglycan syndecan-1 (CD138) in delayed-type hypersensitivity. *J Immunol* 2009;**182**(8):4985-4993.
15. Averbeck M, Gebhardt C, Anderegg U, Termeer C, Sleeman JP, Simon JC. Switch in syndecan-1 and syndecan-4 expression controls maturation associated dendritic cell motility. *Exp Dermatol* 2007;**16**(7):580-589.
16. Stepp MA, Gibson HE, Gala PH, Iglesia DD, Pajoohesh-Ganji A, Pal-Ghosh S, et al. Defects in keratinocyte activation during wound healing in the syndecan-1-deficient mouse. *J Cell Sci* 2002;**115**(Pt 23):4517-4531.
17. Staite ND, Justen JM, Sly LM, Beaudet AL, Bullard DC. Inhibition of delayed-type contact hypersensitivity in mice deficient in both E-selectin and P-selectin. *Blood* 1996;**88**(8):2973-2979.
18. Kinashi T. Overview of integrin signaling in the immune system. *Methods Mol Biol* 2012;**757**:261-278.
19. Yin X, Truty J, Lawrence R, Johns SC, Srinivasan RS, Handel TM, et al. A critical role for lymphatic endothelial heparan sulfate in lymph node metastasis. *Mol Cancer* 2010;**9**:316.
20. Zuberi RI, Ge XN, Jiang S, Bahaie NS, Kang BN, Hosseinkhani RM, et al. Deficiency of endothelial heparan sulfates attenuates allergic airway inflammation. *J Immunol* 2009;**183**(6):3971-3979.
21. Gotte M, Jousen AM, Klein C, Andre P, Wagner DD, Hinkes MT, et al. Role of syndecan-1 in leukocyte-endothelial interactions in the ocular vasculature. *Invest Ophthalmol Vis Sci* 2002;**43**(4):1135-1141.
22. Kiguchi N, Saika F, Kobayashi Y, Kishioka S. Epigenetic regulation of CC-chemokine ligand 2 in nonresolving inflammation. *Biomol Concepts* 2014;**5**(4):265-273.
23. Hauser MA, Schaeuble K, Kindinger I, Impellizzieri D, Krueger WA, Hauck CR, et al. Inflammation-Induced CCR7 Oligomers Form Scaffolds to Integrate Distinct Signaling Pathways for Efficient Cell Migration. *Immunity* 2016;**44**(1):59-72.
24. Morgan MR, Hamidi H, Bass MD, Warwood S, Ballestrem C, Humphries MJ. Syndecan-4 phosphorylation is a control point for integrin recycling. *Dev Cell* 2013;**24**(5):472-485.

25. Hauser MA, Kindinger I, Laufer JM, Spate AK, Bucher D, Vanes SL, et al. Distinct CCR7 glycosylation pattern shapes receptor signaling and endocytosis to modulate chemotactic responses. *J Leukoc Biol* 2016;**99**(6):993-1007.
26. Grabovsky V, Feigelson S, Chen C, Bleijs DA, Peled A, Cinamon G, et al. Subsecond induction of alpha4 integrin clustering by immobilized chemokines stimulates leukocyte tethering and rolling on endothelial vascular cell adhesion molecule 1 under flow conditions. *J Exp Med* 2000;**192**(4):495-506.
27. Johnson LA, Jackson DG. Inflammation-induced secretion of CCL21 in lymphatic endothelium is a key regulator of integrin-mediated dendritic cell transmigration. *Int Immunol* 2010;**22**(10):839-849.
28. Hirose J, Kawashima H, Swope Willis M, Springer TA, Hasegawa H, Yoshie O, et al. Chondroitin sulfate B exerts its inhibitory effect on secondary lymphoid tissue chemokine (SLC) by binding to the C-terminus of SLC. *Biochim Biophys Acta* 2002;**1571**(3):219-224.
29. Kokenyesi R, Bernfield M. Core protein structure and sequence determine the site and presence of heparan sulfate and chondroitin sulfate on syndecan-1. *J Biol Chem* 1994;**269**(16):12304-12309.
30. de Paz JL, Moseman EA, Noti C, Polito L, von Andrian UH, Seeberger PH. Profiling heparin-chemokine interactions using synthetic tools. *ACS Chem Biol* 2007;**2**(11):735-744.
31. Rops AL, Gotte M, Baselmans MH, van den Hoven MJ, Steenbergen EJ, Lensen JF, et al. Syndecan-1 deficiency aggravates anti-glomerular basement membrane nephritis. *Kidney Int* 2007;**72**(10):1204-1215.
32. Weber M, Hauschild R, Schwarz J, Moussion C, de Vries I, Legler DF, et al. Interstitial dendritic cell guidance by haptotactic chemokine gradients. *Science* 2013;**339**(6117):328-332.
33. Clausen BE, Stoitzner P. Functional Specialization of Skin Dendritic Cell Subsets in Regulating T Cell Responses. *Front Immunol* 2015;**6**:534.
34. Ishikawa T, Kramer RH. Sdc1 negatively modulates carcinoma cell motility and invasion. *Exp Cell Res* 2010;**316**(6):951-965.
35. Vuoriluoto K, Hognas G, Meller P, Lehti K, Ivaska J. Syndecan-1 and -4 differentially regulate oncogenic K-ras dependent cell invasion into collagen through alpha2beta1 integrin and MT1-MMP. *Matrix Biol* 2011;**30**(3):207-217.
36. Zong F, Fthenou E, Mundt F, Szatmari T, Kovalszky I, Szilak L, et al. Specific syndecan-1 domains regulate mesenchymal tumor cell adhesion, motility and migration. *PLoS One* 2011;**6**(6):e14816.
37. Hassan H, Greve B, Pavao MS, Kiesel L, Ibrahim SA, Gotte M. Syndecan-1 modulates beta-integrin-dependent and interleukin-6-dependent functions in breast cancer cell adhesion, migration, and resistance to irradiation. *FEBS J* 2013;**280**(10):2216-2227.
38. Ibrahim SA, Yip GW, Stock C, Pan JW, Neubauer C, Poeter M, et al. Targeting of syndecan-1 by

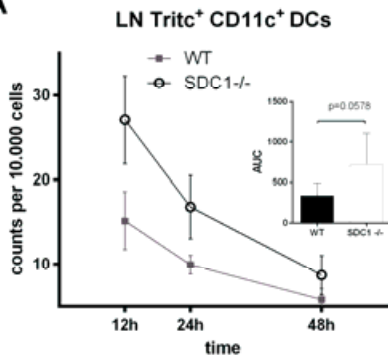
microRNA miR-10b promotes breast cancer cell motility and invasiveness via a Rho-GTPase- and E-cadherin-dependent mechanism. *Int J Cancer* 2012;**131**(6):E884-896.

39. Rovira-Clave X, Angulo-Ibanez M, Reina M, Espel E. The PDZ-binding domain of syndecan-2 inhibits LFA-1 high-affinity conformation. *Cell Signal* 2014;**26**(7):1489-1499.

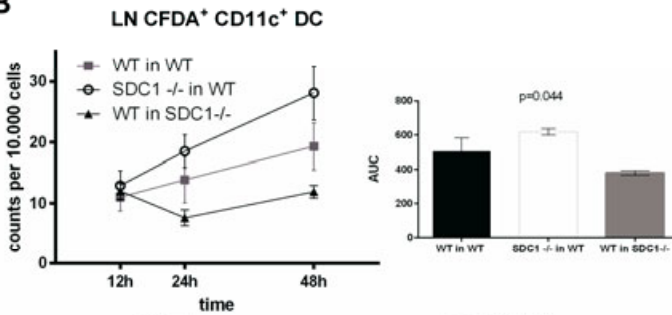
40. Roberts LL, Robinson CM. Mycobacterium tuberculosis infection of human dendritic cells decreases integrin expression, adhesion and migration to chemokines. *Immunology* 2014;**141**(1):39-51.

1

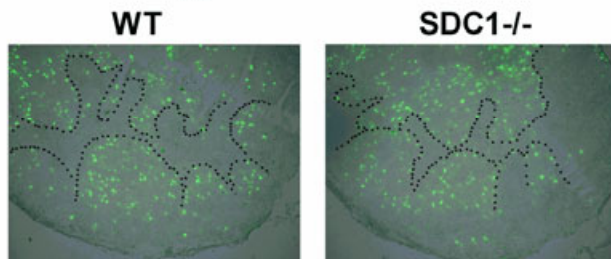
A

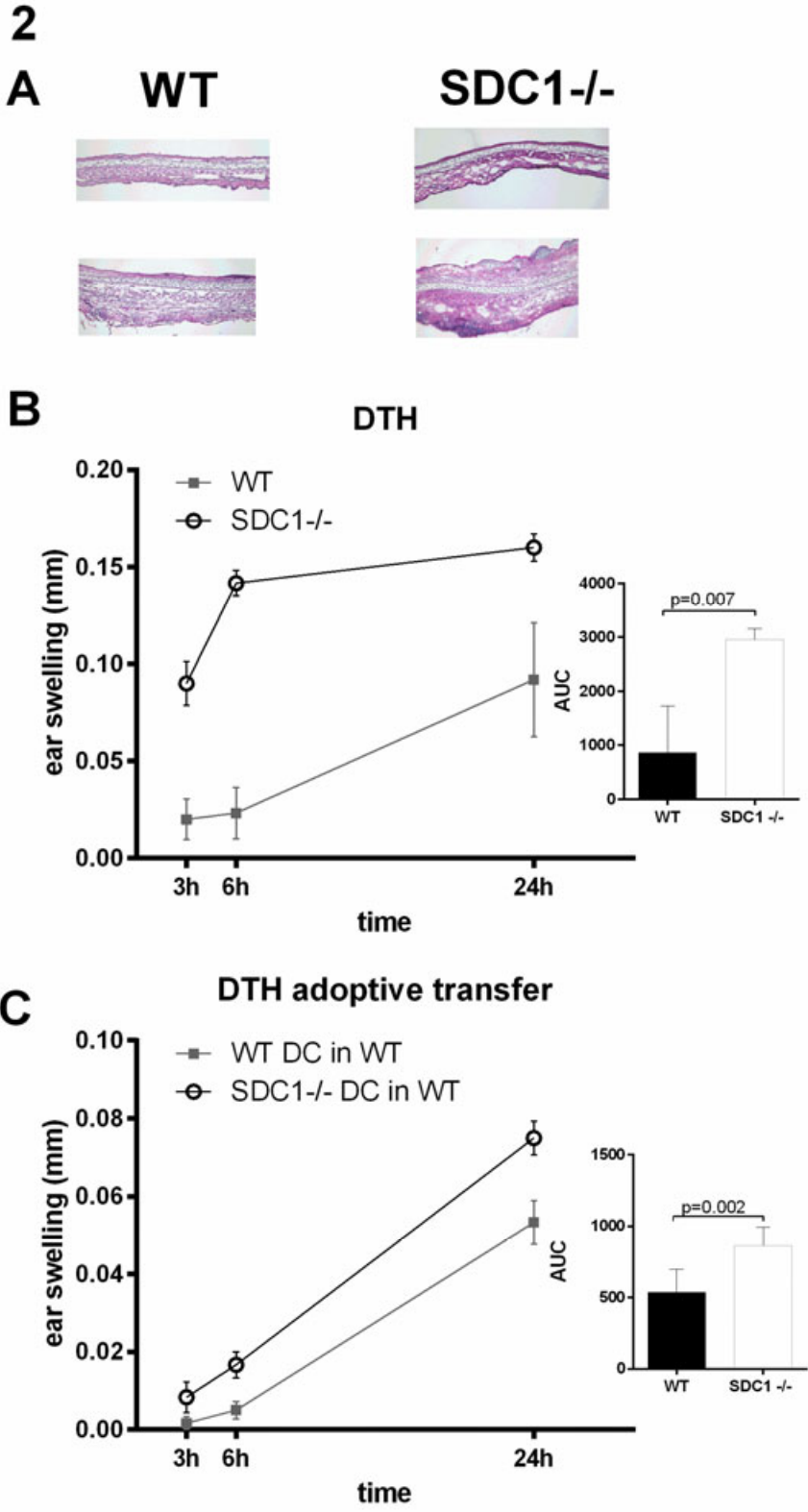


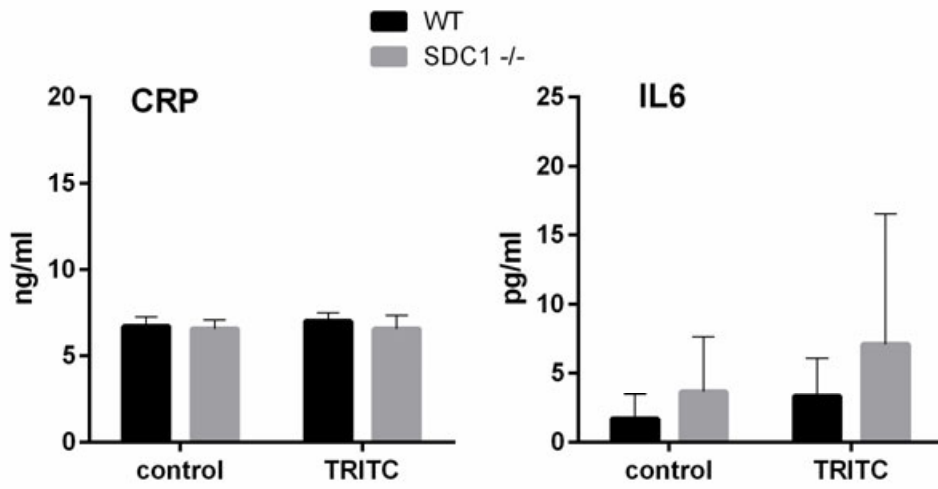
B



C





3
A

B

